

Article

Research on Dynamic Evolution of Residual Stress Based on Simulation of Piston Manufacturing Process

Dong Yang¹, Lizheng Li², Chuanlong Zhou² and Qiang He^{2,*}

¹ Department of Intelligent Equipment, Changzhou College of Information Technology, Changzhou 213164, China

² School of Mechanical Engineering, Jiangsu University of Science and Technology, Zhenjiang 212000, China

* Correspondence: heqiang@just.edu.cn

Abstract: Rather than focusing on the residual stress generated from casting, machining, or heat treatment unilaterally, a comprehensive research method to consider the whole dynamic evolution of residual stress is proposed. The cast iron piston is taken as the research object to establish a continuous simulation model for its manufacturing. Firstly, a simulation model of piston casting is established to analyze the stress change. Subsequently, through the machining and heat treatment simulation of the piston, the variation law of residual stress before and after machining is analyzed. Different process parameters are designed to study the redistribution mechanism of residual stress. Residual stress tests are further conducted on the processed piston products. The results indicate that shakeout can effectively remove 60% to 80% of the residual stress. The removal of materials results in overall residual stress release and redistribution for the piston, and the piston releases 10% to 40% of the residual stress after machining. The heat treatment of the machined piston can effectively reduce the residual stress with a maximum reduction of 27.1%. The good consistency between experimental results and simulation results further confirms the feasibility of the comprehensive research method. This study is beneficial for achieving low stress manufacturing of pistons and improving their working performance.

Keywords: residual stress; cast iron piston; casting; machining; heat treatment



Citation: Yang, D.; Li, L.; Zhou, C.; He, Q. Research on Dynamic Evolution of Residual Stress Based on Simulation of Piston Manufacturing Process. *Metals* **2024**, *14*, 1327. <https://doi.org/10.3390/met14121327>

Academic Editors: Vladimir Dunić, Miroslav Zivkovic, Nenad Djordjevic and Nenad Gubeljak

Received: 10 October 2024
Revised: 20 November 2024
Accepted: 21 November 2024
Published: 24 November 2024



Copyright: © 2024 by the authors. Licensee MDPI, Basel, Switzerland. This article is an open access article distributed under the terms and conditions of the Creative Commons Attribution (CC BY) license (<https://creativecommons.org/licenses/by/4.0/>).

1. Introduction

Cast iron pistons are one of the core components of marine diesel engines, and their complex structure and harsh working environment require high reliability and dimensional accuracy during service [1]. The release of residual stress runs through the entire manufacturing process of the piston, which can be roughly divided into three stages: casting, machining, and heat treatment. The presence of residual stress directly affects the strength and stiffness of the piston, and then reduces its service life [2–4]. Therefore, it is necessary to study the residual stress during the manufacturing process in order to achieve low stress manufacturing, and further improve the working performance of the piston.

In order to study the residual stress in the casting stage, some scholars have studied the development process of stress during casting solidification from the point of view of establishing a theoretical model [5,6]. The pouring temperature affects the liquid fluidity. High pouring temperatures can result in defects, such as porosity and cold segregation, while low pouring temperatures may lead to issues like shrinkage holes [7,8]. Li et al. [9] explored the optimal parameter combination for casting temperature, knockout temperature, and mold preheating temperature in the casting process to mitigate residual stress. Residual stress is one of the important factors affecting the properties of castings. In the process of casting manufacturing, the cooling rate of the adjacent area of the part is also different because of the different wall thickness, which leads to the stress concentration [10–12]. Zhang et al. [13] investigated and continuously optimized the low-pressure casting process

for a ZL205A alloy hemisphere shell casting. Hu et al. [14] established a mathematical model of a continuous casting process to predict the stress change in the casting embryo.

For thin-walled parts, the machining process is mainly achieved by removing the surface materials of the parts. In this process, the initial stress balance is broken, which leads to the redistribution of the stress field, so it is of great significance to study the influence of machining residual stress on machining quality and mechanical properties [15–17]. Jiang et al. [18] found that the tensile residual impact stress on the machined surface can be reduced by increasing the cutting speed. The increase in cutting speed will lead to a higher temperature and smaller force. High temperatures can release the internal stress of the material, and a small force may reduce the deformation and stress concentration of the workpiece, thereby reducing the accumulation of residual stress. Zhang et al. [19] studied the coupling distribution of initial residual stress and machining residual stress and found that the influence of coupling stress distribution is very significant with the decrease in the thickness of thin-walled parts. Huang et al. [20] comprehensively considers the mechanism of the influence of machining parameters and tool parameters on residual stress.

More importantly, Jiang et al. [21] studied the redistribution of residual stress on the surface during machining and found that the overlapping effect of cutting tools has an important influence on the deformation of thin-walled parts. Robinson et al. [22,23] analyzed the redistribution of residual stress in aluminum alloy 7449 during layer-by-layer removal. Zhou et al. [24] et al. proposed a novel genetic-based residual stress and deformation prediction method for the coupled machining process of connecting rods. In Guo et al. [25], in order to study the effect of residual stress on the deformation of thin-walled parts, the redistribution mechanism of residual stress in the grinding process was analyzed.

Heat treatment is a technological process in which the internal stress is released over time by placing the part at a higher temperature in order to reduce the residual stress of the part. Some scholars [26–28] use the traditional inverse heat transfer method to determine the actual heat transfer coefficient of parts during quenching and carry out numerical simulations of quenching. The results show that the process parameters have an important influence on the residual stress. Dong et al. [29] studied the effects of different quenching temperatures and hot and cold cycles on residual stress. Zhang et al. [30] studied the effect of cooling rate on the residual stress and tensile properties of aluminum alloy. In addition, some scholars focus on the influence of the structure and materials of heat-treated parts on residual stress [31]. Kaiser et al. [32] found that short-time quenching and tempering will lead to the transformation of surface residual stress from compressive stress to tensile stress. Li et al. [33] analyzed the superimposed residual stresses produced by heat treatment and grinding processes and found that the heat treatment and grinding processes produce compressive residual stresses.

However, the above studies only focused on the residual stress generated from casting, machining, or heat treatment unilaterally; the research on the dynamic evolution of residual stress is more important. Su et al. [34] introduced residual stress generated by casting as the initial conditions for a heat-treated step part of 4140 steel. Tian et al. [35] proposed a comprehensive research method to consider the whole dynamic evolution of the casting from the residual stress generated by casting to the stress relief by heat treatment.

It is crucial to study the residual stress during the manufacturing process in order to achieve low stress manufacturing and further improve the working performance of the piston. In this paper, rather than focusing on the residual stress generated from casting, machining, or heat treatment unilaterally, a comprehensive research method to consider the whole dynamic evolution of residual stress is proposed. The cast iron piston is taken as the research object to establish a continuous simulation model for its manufacturing. The simulation model of piston casting is established to analyze the stress change in the process of casting. The change law of the residual stress before and after machining is further analyzed based on the simulation model of piston machining and heat treatment. Meanwhile, the effect of heat treatment on reducing and homogenizing the residual stress of

the piston is explored. The influence of different process parameter conditions is analyzed by numerical simulation, and we explore the redistribution mechanism of residual stress in the piston manufacturing process. Residual stress tests are further conducted on the processed piston products to confirm the feasibility of the comprehensive research method.

2. Materials and Methods

2.1. Workpiece Material

The working environment of a marine diesel engine piston requires it to have the characteristics of high strength, high toughness, and high wear resistance. The material used in actual production is nodular cast iron QT700. The iron QT700 has the same material composition as EN-GJS-700 in software ProCAST 2019, and the software provides the required thermal properties parameters for casting. Its chemical composition is shown in Table 1. The stress data are based on the built-in Linear Elastic in the software material library, and the sandbox material is selected as Green Sand. The mold cavity is defined as 100%, and the stress data are rigid. Because this study mainly considers the influence of pouring temperature and sand dropping temperature on the residual stress of the piston, complete rigidity can well represent the influence of pouring temperature and sand dropping temperature on the residual stress of the piston, as well as the process of stress and strain changes. At the same time, due to the fact that the fully rigid sandbox model can ignore the calculation of stress, the calculation speed is improved. To further simulate mechanical processing and heat treatment processes in ABAQUS 2016, Table 2 just shows the material parameters of QT700 shown after further interpolation processing, and the units in the table need to be converted to the units input into ABAQUS accordingly.

Table 1. Chemical composition of QT700.

C	Cu	Mg	Mn	Si	P	S
3.5	0.8	0.06	0.1	2.7	<0.05	<0.05

Table 2. Material parameters.

T (°C)	ρ (kg/m ³)	E (GPa)	μ	C_p (J·(kg ⁻¹ ·K ⁻¹))	α (10 ⁻⁵ K ⁻¹)	K (W·m ⁻¹ ·K ⁻¹)
20	7.44×10^3	103.479	0.28	445	2.05	44
100	7.33×10^3	103.478	0.28	443	2.05	45
300	7.16×10^3	100.632	0.28	484	2.04	37
500	7.13×10^3	84.193	0.28	530	2.04	27
700	7.04×10^3	60.431	0.28	624	1.90	29

2.2. Multi-Process Simulation Modeling

The basic structure of the piston is cylindrical, the material is QT700, the maximum diameter is $\varnothing 280$ mm, the overall height is 330 mm, the net weight 54 Kg, the maximum wall thickness is 33 mm, and the minimum wall thickness is 12 mm. There are two pin holes with diameters of $\varnothing 120$ mm on the side wall of the casting, which are typical thin-wall castings. The three-dimensional model is shown in Figure 1a. According to the structural characteristics and casting process of the piston, the gating system model is determined, as shown in Figure 1b.

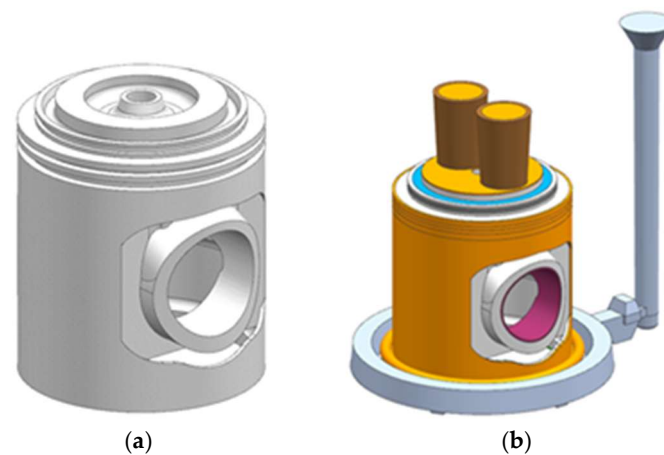


Figure 1. Establishment of 3D models: (a) Piston model (b) Pouring system model.

In the three-dimensional modeling stage of the piston, the model needs to be processed, and the materials that need to be removed in the subsequent machining simulation are drawn into a single part, and finally a complete assembly model is formed with the piston model and the gating system model. The assembled casting system model is imported from the three-dimensional software UG NX 2021 to ProCAST 2019 for meshing, and the finite element model is shown in Figure 2. The Visual Mesh module of ProCAST software is used to partition the mesh size. The mesh size of the gating system and the casting mesh size are both 6 mm. The number of elements in the model is 1,455,287, and the mesh type is C3D4 (tetrahedral elements).

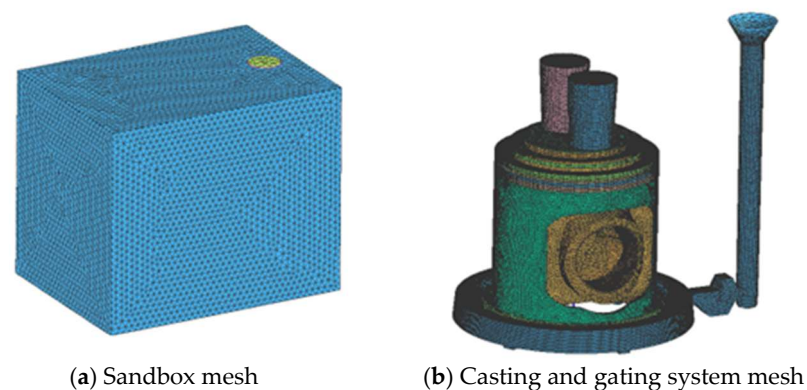


Figure 2. Finite element model: (a) Sandbox mesh; (b) Casting and gating system mesh.

The gravity casting process is adopted in the actual production of cast iron pistons. The casting simulation needs a pouring time of 7 s, a pouring temperature of 1430 °C, and an initial sandbox temperature of 25 °C. After the pouring is completed, the liquid metal fills the mold cavity and carries out heat transfer, and the thermal boundary condition between the sandbox and the air is set to air cooling. The top wall thickness of the casting is relatively large, and the side wall thickness is uneven. Therefore, it is required that the metal liquid rises steadily and slowly along the mold cavity during the filling process. At the same time, according to the principles of simultaneous solidification and equilibrium solidification, in order to reduce the temperature field during the solidification process of casting, the casting method is determined to be a bottom pouring system. The casting adopts a semi-closed pouring system, and the minimum flow resistance section size should be firstly determined when designing the dimensions of each runner. Meanwhile, the calculation of the dimensions of each sprue in the pouring system should use the inner sprue section size as the minimum section reference, which is beneficial for ensuring the rapid filling of the molten metal. The cross-sectional ratio of the inner runner, transverse

runner, and straight runner is $A1:A2:A3 = 1:1.5:1.2$, and the inner runners are dispersed and arranged at the bottom of the casting. The shrinkage feeders are added at the locations where casting defects may occur to supplement the solidification process of the casting.

After the pouring is completed, the liquid metal fills the mold cavity and carries out the heat transfer, and the thermal boundary condition between the sandbox and the air is set to air cooling. The heat transfer coefficient between the casting and the mold is set to $800 \text{ W}/(\text{m}^2 \cdot \text{K})$ before the solidification of the molten metal; after the solidification of the molten metal, the heat transfer coefficient between the casting and the mold is $400 \text{ W}/(\text{m}^2 \cdot \text{K})$. The heat transfer coefficient between the mold and the air contact surface is set to $10 \text{ W}/(\text{m}^2 \cdot \text{K})$.

The cast iron piston retains a certain amount of casting residual stress in the casting stage. After a large number of materials are removed in the machining process, the release and redistribution of the original residual stress in the casting is the main reason for the deformation of the workpiece in the machining process. The machining process of the piston machine is shown in Table 3.

Table 3. Simplified process flow.

Serial Number	Process Name
1	Car end face
2	Outer circle of car
3	Drill hole
4	Boring
5	Car combustion chamber
6	Ring groove

Before piston machining simulation, the casting residual stress simulated by ProCAST software should be loaded onto the finite element model of piston machining in ABAQUS software. The specific implementation method is as follows: the ABAQUS keyword is edited, adding *InitialConditions, type = stress, and input = cast.dat statements between *Material and Step. The “life and death unit” technology is used to simulate the machining process of the piston to achieve the removal of metal materials.

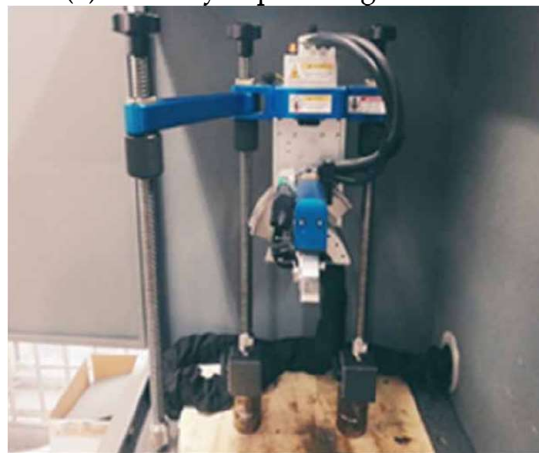
Finally, in order to reduce and homogenize the residual stress, stress relief annealing is carried out for the complex structure of the parts, while stress relief annealing heat treatment mainly includes three processes: the heating, insulation, and cooling processes. The machined workpiece is placed in the heat treatment furnace, and the workpiece is heated from room temperature to a certain temperature according to the appropriate heating speed. After reaching this temperature and holding the heat for a period of time, cooling is performed with the furnace to a certain temperature at the appropriate cooling speed, and finally the air is cooled to room temperature. The specific process flow is as follows: heating to $580 \text{ }^\circ\text{C}$, holding the heat for 3 h, cooling to $200 \text{ }^\circ\text{C}$ with the furnace, and natural air cooling to $25 \text{ }^\circ\text{C}$, where the heating and cooling speeds are not less than $50 \text{ }^\circ\text{C}/\text{h}$.

2.3. Experimental Setup

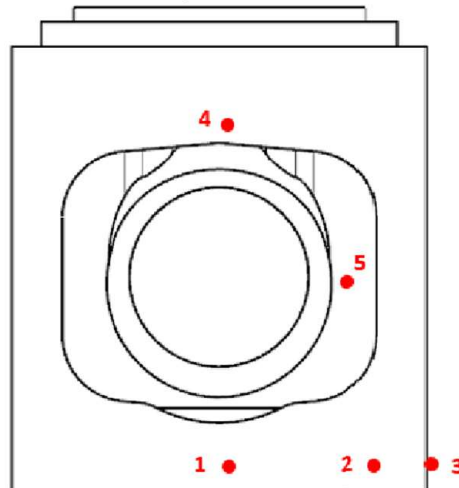
The rationality of the piston multi-process continuous simulation model is verified by the residual stress test experiment. The X-ray stress detector Xstress3000G2 and the electrolytic polishing machine XF-1 selected by the experimental instrument are shown in Figure 3a,b. Figure 3c is a schematic diagram of the piston measuring point. Considering the structural characteristics of the piston, the selection of the five measuring points is mainly concentrated around the piston pin hole and skirt, in which measuring points 1, 2, and 3 are distributed in the piston skirt, and measuring point 4 is located on the upper side of the pin hole, while measuring point 5 is located on the side plate. In addition, because the X-ray inspection has some requirements on the surface quality of the tested sample, it is necessary to carry out electrolytic polishing on the testing point.



(a) Electrolytic polishing machine



(b) X-ray stress detector



(c) Schematic diagram of piston measuring point

Figure 3. Test arrangement. (a) Electrolytic polishing machine; (b) X-ray stress detector; (c) Schematic diagram of piston measuring point.

In order to ensure the accuracy and reliability of the experimental data, the piston parts used in the measurement are all pistons produced in the same batch, 5 groups of pistons in each process stage are selected, and the average number of 5 groups of experimental results is taken. The physical figure of the selected piston after machining and heat treatment is shown in Figure 4.

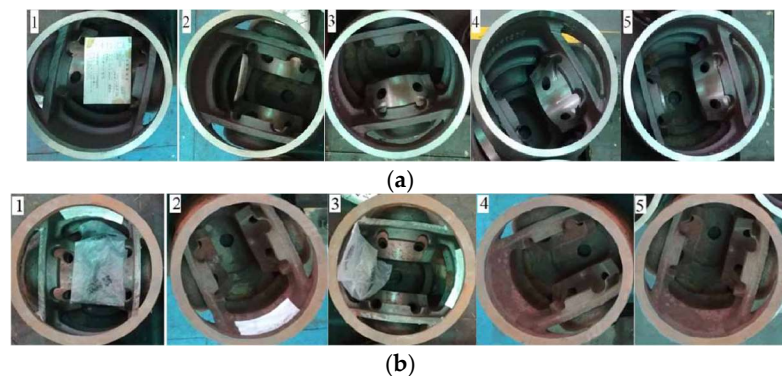


Figure 4. Physical image of the test piston: (a) Piston after machining; (b) Piston after heat treatment.

3. Results and Discussion

3.1. Casting Simulation Results

With the solidification process, a temperature difference between the inner and outer layers and an uneven distribution of temperature in different regions of the casting will appear. The metal liquids in different parts will obstruct each other when contracting, leading to the generation of thermal stress. In addition, the blocking effect of the sandbox on the casting shrinkage will also lead to casting forces, which will form a stress field in the casting.

The restraint of the sandbox is lost after the sand falls, and the overall stress of casting decreases greatly. When the piston castings are cooled in air, the stress increases slowly with the decrease in temperature, and gradually tends to a stable value. Figure 5a shows the stress nebulae of the piston during shakeout. It can be seen from the figure that the residual stress of the whole piston at this time is mainly concentrated in 70~250 MPa, and the stress is mainly distributed in the piston head, pin hole side plate, and skirt area, among which the maximum stress in the side plate and skirt area is about 250 MPa. Figure 5b shows the stress cloud diagram of the piston when it cools down to room temperature. At this time, the piston loses the restraint effect of the sandbox, and the overall stress begins to change and transfer. It can be seen from the figure that the residual stress of the piston castings is not high and is mostly kept in the range of 25~115 MPa. The residual stress is mainly concentrated in the top, head, pin hole, side plate, and skirt of the casting. The main reason is that the wall thickness of the top, head, and pin hole of the casting is large, and the temperature difference between the inner and outer surface is large during the cooling process, which causes the stress concentration. The residual stress of the side plate and the skirt is caused by the cooling deformation of thin-wall thickness. The maximum residual stress of casting does not exceed the tensile strength of the material.

Figure 6a shows the stress variation curve of measuring points 1–5 from the beginning of the solidification of the casting to the sand falling. From the graph, it can be seen that the stress changes in measuring points 1–5 during the cooling process are basically consistent, and can be roughly divided into three stages: the stage of rapid stress growth at the beginning of solidification, the stage of stress reduction, and the stage of gradually increasing stress with cooling. At the beginning of solidification, the liquid metal in the sandbox has good shrinkage and deformation ability, and there is no stress generated at this time. As the temperature decreases, the molten metal begins to cool and solidify, and the liquid phase inside the casting gradually begins to transform into a solid phase. The ratio of the solid phase continues to increase, and the mutual hindrance and confinement of the sandbox inside the casting lead to a rapid increase in stress. As the casting gradually solidifies and undergoes phase transformation, its volume gradually increases. The hindering effect inside the casting decreases, and the stress decreases accordingly. After the casting is completely solidified, the stress of the casting is mainly affected by the cooling rate in each region. As the temperature difference in each region decreases, the stress slowly increases. Points 1, 2, and 3 in the figure have similar wall thicknesses and are located in the piston

skirt, so the stress changes in the three stages are basically the same. However, points 4 and 5 are affected by wall thickness and position, and the stress reduction stage and stress gradually increasing stage with cooling occur later than points 1, 2, and 3. Figure 6b is the stress change curve of the casting at measuring points 1~5 when the casting is cooled to room temperature after sand outfall. It can be seen from the figure that the constraint effect of the sandbox is lost after sand outfall, and the stress at each point of the casting decreases significantly in a short time. Subsequently, the castings were cooled in the air, and the stress in each region rose slowly due to different local cooling rates. After a period of time, the stress growth at each point tended to be flat. The stress growth of point 5 is larger than other points due to the tensile action of the pin hole and piston skirt on both sides.

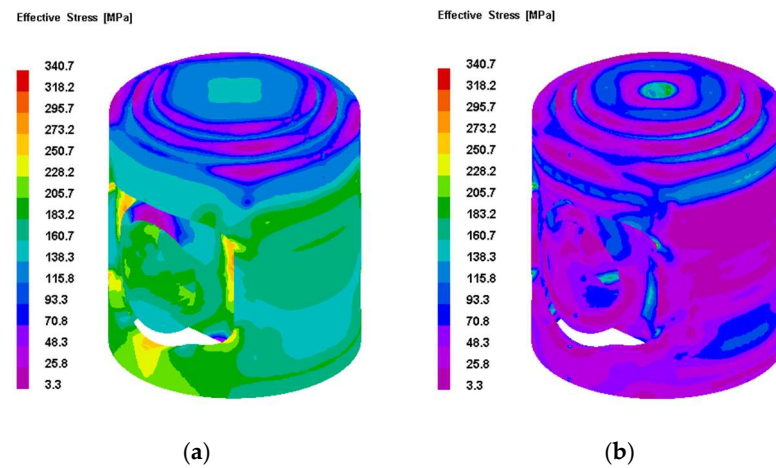


Figure 5. Cloud chart of residual stress in piston casting: (a) Residual stress before shakeout; (b) Residual stress after shakeout.

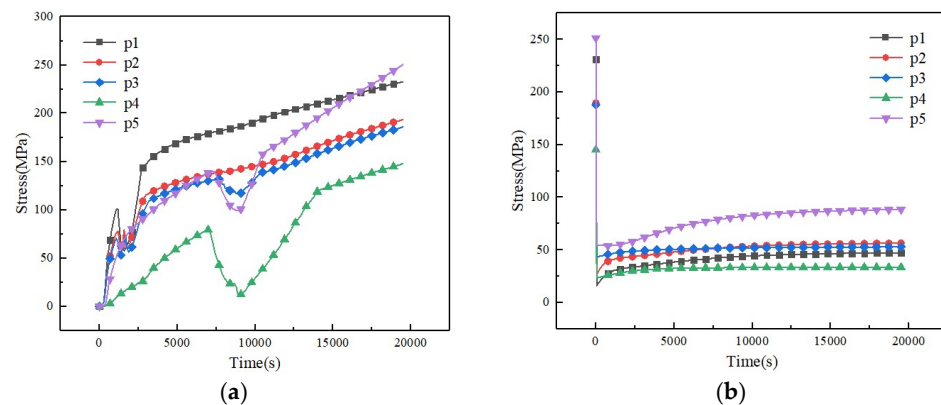


Figure 6. Stress CHANGE curve at measurement point: (a) Stress change curve before shakeout; (b) Stress change curve after shakeout.

3.2. Machining Simulation Results

The residual stress of castings after sand falling out at 500 °C is taken as the initial residual stress of piston machining simulation. The piston machining simulation is carried out according to the piston machining process in Table 4. The stress nebulogram of the piston before and after machining simulation is shown in Figure 7.

Table 4. Different shakeout temperature parameters.

Factor	Shakeout Temperature (°C)
A	300
B	400
C	500
D	600

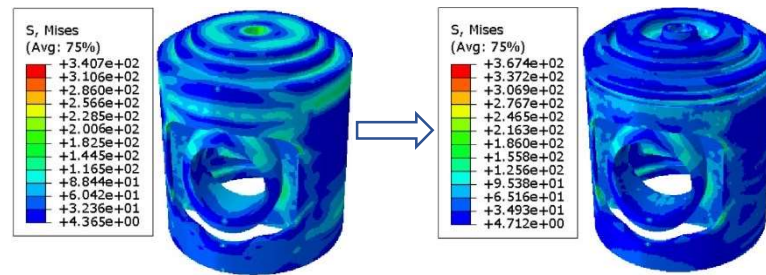


Figure 7. Stress cloud diagram before and after piston processing.

It can be seen from Figures 7 and 8 that the casting residual stress is taken as the initial stress. After the machining simulation of the piston, the overall residual stress of the piston begins to be redistributed and released due to the removal of materials in various parts. The stress of the piston is mainly concentrated on the top surface, the top step, the outer circle, the side plate and the pin hole before machining. The residual stress at the top of the piston is transferred to the inner wall of the combustion chamber after removing the combustion chamber material. The residual stress at the top step and ring groove is transferred to the processed surface of the ring groove. The residual stress at the outer circle, side plate, and pin hole decreases or increases to varying degrees. Taking the measuring points at the outer circle of the piston and the rib as an example, it can be seen from Figure 8 that the residual stress at points 1 and 3 is increased after machining, while the residual stress at points 2, 4, and 5 is reduced to different degrees, and the stress release at point 2 is reduced by 45.1% compared with that before machining.

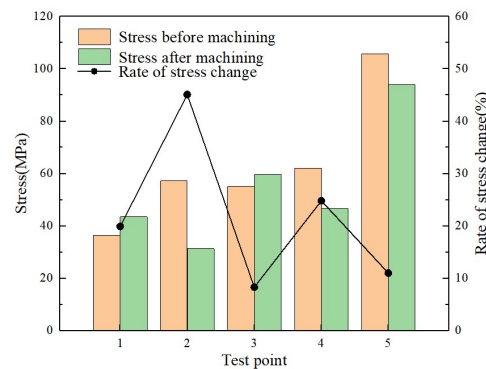


Figure 8. Stress changes at each measurement point.

3.3. Simulation Results of Heat Treatment

The machined piston was annealed for stress removal, heated at 80 °C/h, kept at 560 °C for 3 h, and finally cooled in the furnace at 40 °C/h. The overall temperature of the piston increases gradually, and the yield strength of the piston decreases with the increase in temperature. When the yield strength of the material is lower than the residual stress in the piston, plastic deformation will occur in the local area of the piston structure, and certain residual stress will be released. The stress distribution during the stress removal annealing process is shown in Figure 9. Heat treatment can eliminate part of the residual stress, but

cannot completely eliminate the residual stress; the heat treatment of the machined piston can effectively reduce the residual stress, and the maximum residual stress is reduced by 24.1%.

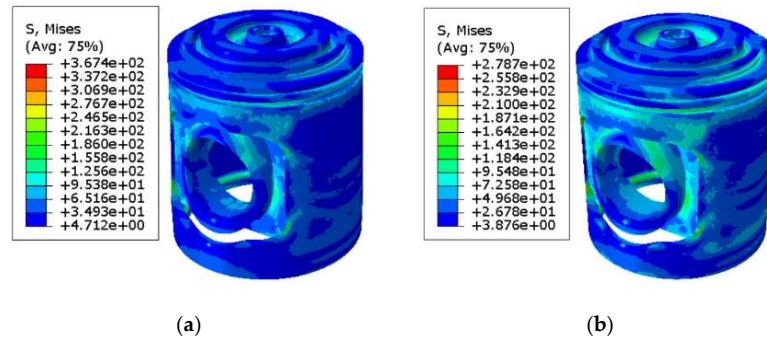


Figure 9. Stress distribution before and after heat treatment: (a) Before heat treatment; (b) After heat treatment.

3.4. Effect of Process Parameters on Residual Stress

3.4.1. Effect of Shakeout Temperature on Residual Stress

The shakeout temperature is an important factor affecting the residual stress of castings. The castings after shakeout are cooled in the air, and the choice of temperature will affect the cooling rate of the castings, thus affecting the residual stress when the castings are cooled to room temperature. This section will study the effect of different shakeout temperature on the residual stress of castings, and the shakeout temperature parameters are shown in Table 4.

It can be seen from Figure 10 that after removing the sandbox, the maximum residual stress of the casting decreases from 470 MPa at 300 °C to 276.2 MPa at 600 °C with the increase in shakeout temperature. The higher the shakeout temperature is, the smaller the maximum residual stress is. Figure 11 shows the stress variation diagram of measuring points 1 to 5 with the shakeout temperature. The stress of five measuring points is the highest at 300 °C, and the residual stress is the lowest at 600 °C, while the residual stress is the largest after shakeout at 600 °C. With the increase in the shakeout temperature, the cooling rate of the casting increases rapidly in a short time, and the local temperature difference in the casting increases, so that the residual stress increases after the shakeout and the stress decreases gradually before the shakeout. The residual stress increases gradually.

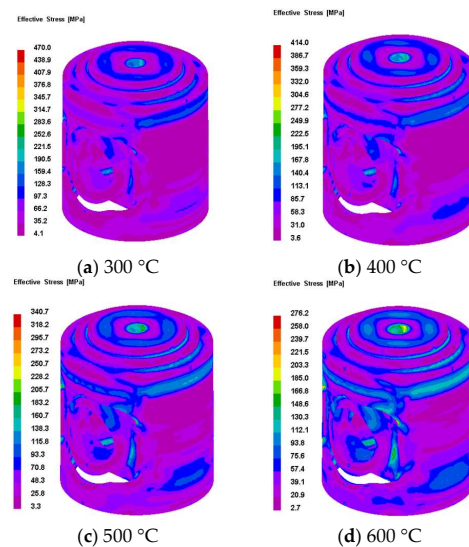


Figure 10. Stress nephogram under different shakeout temperatures.

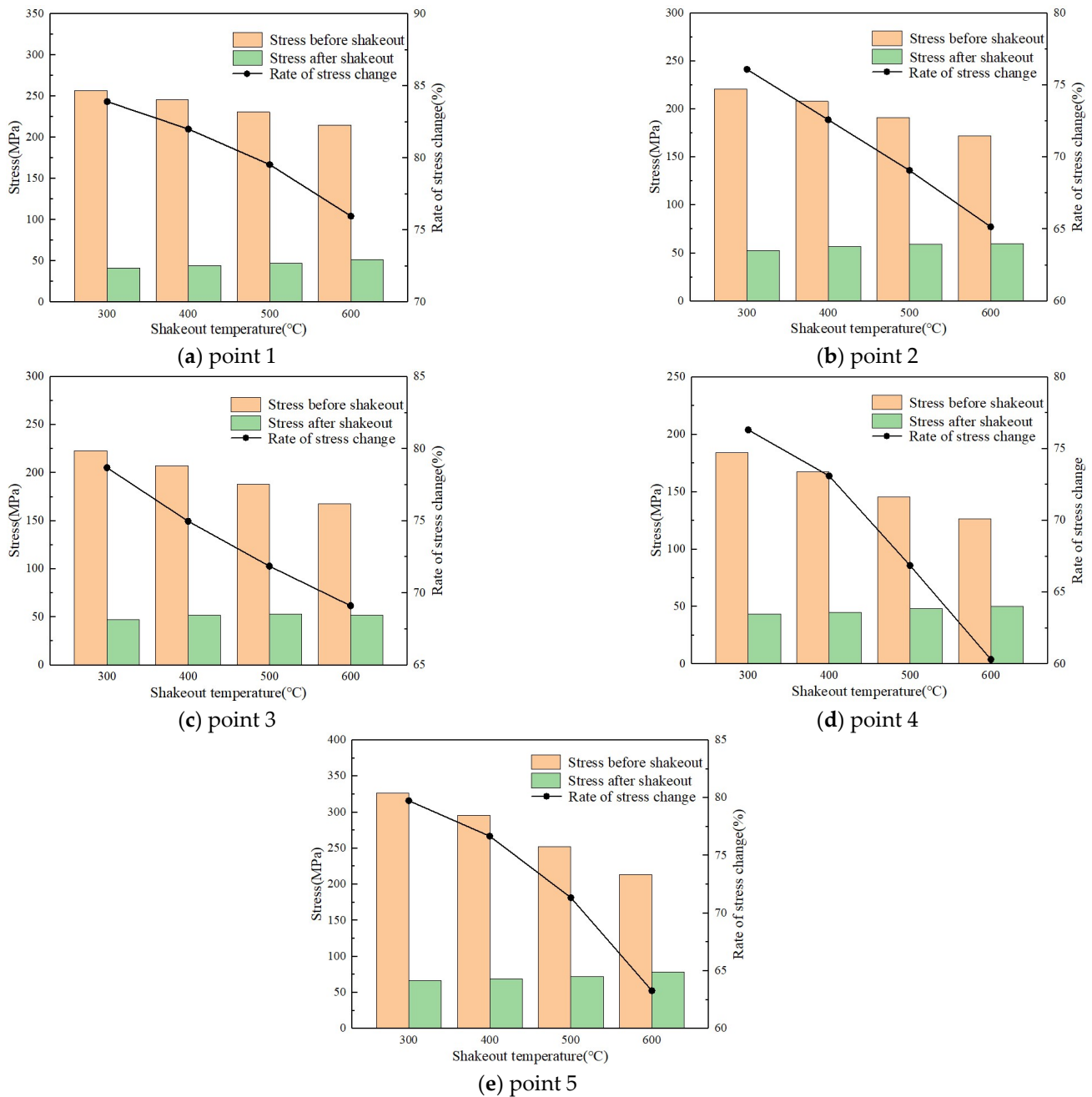


Figure 11. Stress changes at various points under different shakeout temperatures.

3.4.2. Effect of Initial Stress on Residual Stress

The casting residual stress at the shakeout temperatures of 300 °C, 400 °C, 500 °C, and 600 °C is taken as the initial stress of piston machining, and the processing technology in Table 3 is selected. The stress changes in each area of the piston with different initial stresses after different shakeout temperatures are shown in Figure 12. As can be seen from the diagram, the stress change trend in the piston under different initial stress conditions is basically the same under the same processing technology. After machining, the stress in each area of the piston increases and decreases in different magnitudes: the residual stress in the combustion chamber area after piston processing increases with the shakeout temperature, and the stress increase trend in the combustion chamber area decreases gradually in the range of 300 °C to 500 °C. Under the condition of shakeout at 500 °C, the stress in the piston combustion chamber undergoes no obvious change before and after

processing, but the stress begins to decrease when the shakeout temperature exceeds 500 °C. With the increase in the shakeout temperature, the stress in the piston head area decreases after machining, and the higher the temperature is, the greater the stress decreasing trend is; the stress in the pin hole area has no significant change before the shakeout temperature reaches 500 °C. When the shakeout temperature reaches 600 °C, the stress increases by 16.73% before and after processing, and the decreasing trend in stress in the side plate decreases with the increase in shakeout temperature. In the range of 300 °C to 600 °C, the shakeout temperature has little effect on the increasing trend in stress of the piston skirt. Under different initial stress conditions, the stress influence of machining on each region of the piston is as follows: head area > skirt area > pin hole area > side plate area > combustion chamber area.

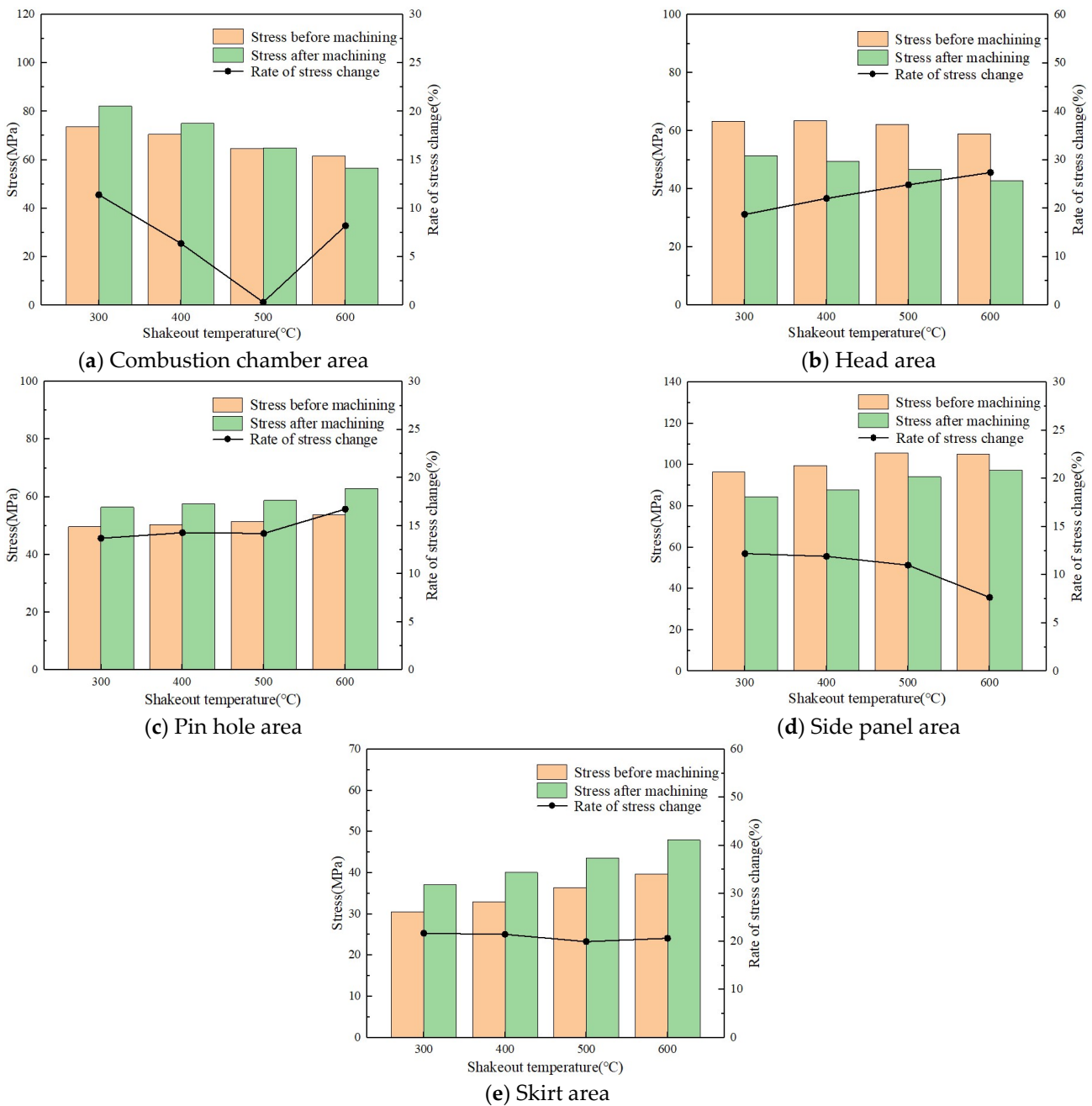


Figure 12. Stress changes in various regions under different initial stresses.

3.4.3. Effect of Holding Temperature on Residual Stress

In order to study the effect of different holding temperatures on the residual stress of piston machining, the specific process parameters are shown in Table 5.

Table 5. Different insulation temperature parameters.

Factor	Insulation Temperature (°C)
A	540
B	560
C	580
D	600

Figure 13 shows the cloud map of residual stress distribution at different insulation temperatures. The heating speed, holding time, and cooling rate remain unchanged during each simulation. In the process of annealing, with the increase in insulation temperature, the residual stress of the piston decreases continuously, and the effect of different insulation temperatures on stress relief is different. The maximum stress of the piston decreases from 367.4 MPa to 270.9 MPa at 540 °C and from 367.4 MPa to 233.3 MPa at room temperature. Therefore, when the insulation temperature changes between 540 °C and 600 °C, compared with other factors, the insulation temperature has a significant effect on the elimination of residual stress.

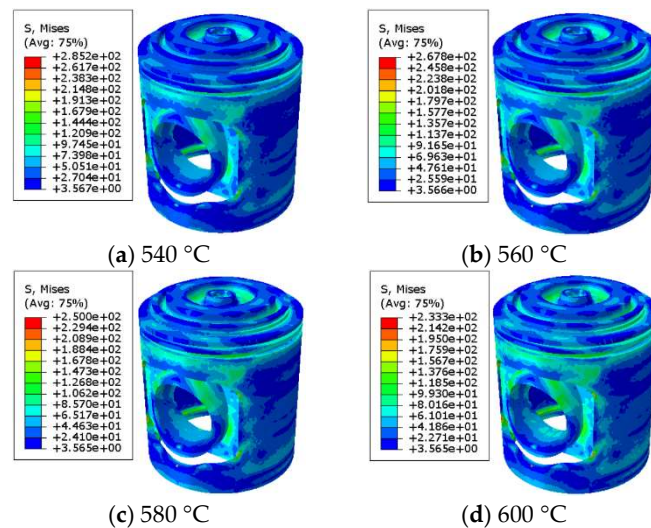


Figure 13. Residual stress distribution at different insulation temperatures.

It can be seen from Table 6 that when the insulation temperature increases within a specific range, the reduction effect of residual stress is also enhanced. When the insulation temperature of the piston reaches 580 °C, the internal residual stress has been eliminated by 31.9%. However, when the insulation temperature continues to increase to 600 °C, the elimination of residual stress by insulation temperature begins to weaken.

Table 6. Residual stress relief effect under different insulation temperatures.

Order	Insulation Temperature (°C)	Stress Value (MPa)		Relief Percentage
		Before Heat Treatment	After Heat Treatment	
1	540	367.4	285.2	22.3%
2	560		267.8	27.1%
3	580		250.0	31.9%
4	600		233.3	36.4%

3.5. Verification of Multi-Process Residual Stress of Diesel Engine Piston

Figure 14 shows the residual stress data of the piston surface. It is found that although there are differences between the experimental values and the simulated values of the measuring points on the piston surface, the error between the simulated values and the experimental values of the measuring points is basically within 50 MPa. By analyzing the simulation results and the experimental results, it is found that the difference between the simulation values and the experimental values in the machining stage of piston is large. This is because the surface residual stress caused by the cutting friction of the tool is retained on the surface of the piston parts measured in the experiment after the cutting action of the tool, while the cutting action of the tool is not considered in the machining simulation. The difference between the simulated value and the experimental value of heat treatment is reduced to a certain extent, because after heat treatment, the influence of the residual stress on the surface of the piston parts is weakened, and the stress variation trend in the simulated value and the experimental value is basically the same, which shows that the multi-process continuous simulation of the piston is reliable.

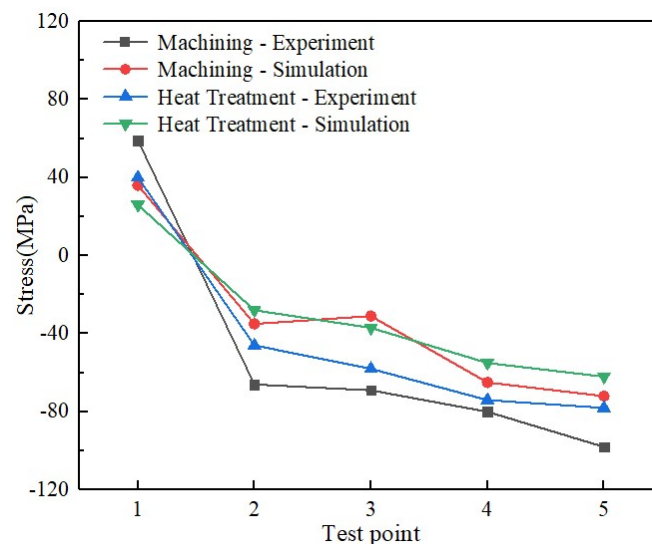


Figure 14. Residual stress simulation and test results.

4. Conclusions

In this paper, aiming at the manufacturing process of a marine diesel engine piston, the multi-process continuous simulation process of the piston from casting to machining to heat treatment is established. The variation law of residual stress in the piston manufacturing process is studied, which is of theoretical significance and engineering application value for optimizing the manufacturing process and the process parameters of pistons.

Before shakeout, the casting stress is mainly concentrated in the thin-walled area, but after shakeout, the stress is redistributed, and the casting stress is mainly concentrated in the wall thickness area, and shakeout can effectively remove 60% to 80% of the residual stress. With the increase in shakeout temperature, the stress of castings decreases gradually before shakeout, while the residual stress increases gradually after shakeout.

Taking the residual stress after shakeout as the initial stress, and considering the clamping technology, the residual stress in the machining stage of piston machining is studied. The removal of materials results in the overall residual stress release and redistribution of the piston, and after machining, the piston releases 10% to 40% of the residual stress. The heat treatment of the machined piston can effectively reduce the residual stress, and the maximum residual stress is reduced by 27.1%.

Author Contributions: Conceptualization, writing—original draft, D.Y.; resources, software, L.L.; writing—review and editing, resources, C.Z.; methodology, software, Q.H. All authors have read and agreed to the published version of the manuscript.

Funding: This work was financially supported by The Natural Science Foundation of the Jiangsu Higher Education Institutions of China (21KJD460001), the National Key Research and Development Program of China (2019YFB1706705) and Natural Science Research Project of Changzhou College of Information Technology (CXZK202107Y). The authors would like to express their thanks.

Data Availability Statement: Data are contained within the article.

Conflicts of Interest: The authors declare there are no conflicts of interest regarding the publication of this work.

References

- Zhang, S.Y.; Ran, Y.; Murphy, A.; Zhang, G.B.; Wang, W. Residual stress analysis of gray cast iron manufacturing processes. *Mater. Manuf. Process.* **2020**, *35*, 1781–1788. [[CrossRef](#)]
- Alipooramirabad, H.; Kianfar, S.; Paradowska, A.; Ghomashchi, R. Residual stress measurement in engine block—an overview. *Int. J. Adv. Manuf. Technol.* **2024**, *35*, 1–27. [[CrossRef](#)]
- Zhao, D.H.; Ai, Z.H.; Liu, Y.L.; Li, G.C.; Zhou, H.G.; Bai, X.X. Evolution analysis of process-induced residual stress during the manufacture of diesel engine block. *Int. J. Adv. Manuf. Technol.* **2022**, *120*, 2655–2669. [[CrossRef](#)]
- Kianfar, S.; Aghaie, E.; Stroh, J.; Sediako, D.; Tjong, J. Residual stress, microstructure, and mechanical properties analysis of HPDC aluminum engine block with cast-in iron liners. *Mater. Today Commun.* **2021**, *26*, 101814. [[CrossRef](#)]
- Ruggiero, A.; Khademi, E. Micromechanical Modeling for Predicting Residual Stress-Strain State around Nodules in Ductile Cast Irons. *Metals* **2023**, *13*, 1874. [[CrossRef](#)]
- Seydani, M.Z.; Krimi, A.; Khelladi, S.; Bedel, M.; El Mansori, M. 3D numerical simulation and experimental validation of resin-bonded sand gravity casting: Filling, cooling, and solidification with SPH and ProCAST approaches. *Therm. Sci. Eng. Prog.* **2024**, *47*, 102329. [[CrossRef](#)]
- Shi, X.A.; Lv, C.H.; Li, G.C.; Wang, K.L.; Chen, J.Z.; Tang, J. Study on induction hardening performance of 34CrNi3MoA steel crankshaft. *Front. Mater.* **2023**, *10*, 1240087. [[CrossRef](#)]
- Cui, Z.X.; Hu, X.D.; Dong, S.Y.; Yan, S.X.; Zhao, X. Numerical simulation and experimental study on residual stress in the curved surface forming of 12CrNi2 alloy steel by laser melting deposition. *Materials* **2020**, *13*, 4316. [[CrossRef](#)]
- Li, G.; Zhou, X.; Zhang, L.; Du, Y.F.; Zhang, D. Dynamic evolution of residual stress upon manufacturing Al-based diesel engine diaphragm. *High Temp. Mater. Process.* **2024**, *43*, 20240032. [[CrossRef](#)]
- Guo, T.; Sun, Q.; Li, K.; Huang, D.; Wang, J.; Tai, X. Effect of temperature gradient and cooling rate on solidification structure and properties of ZL205A alloy. *Rare Met. Mater. Eng.* **2022**, *51*, 2400–2408.
- Dini, H.; Andersson, N.E.; Jarfors, A.E. Effect of process parameters on distortion and residual stress of high-pressure die-cast AZ91D components. *Int. J. Met.* **2018**, *12*, 487–497. [[CrossRef](#)]
- Afazov, S.M.; Becker, A.A.; Hyde, T.H. FE prediction of residual stresses of investment casting in a Bottom Core Vane under equiaxed cooling. *J. Manuf. Process.* **2011**, *13*, 30–40. [[CrossRef](#)]
- Zhang, Z.H.; Liu, J.H.; Chen, J.M.; Wen, F.L.; Jia, R.; Ma, Q.X. Optimization of residual stress in low-pressure casting of ZL205A alloys. *J. Manuf. Process.* **2023**, *99*, 338–350. [[CrossRef](#)]
- Hu, Y.; Li, M.; Hao, H. Development of a mathematical model and its application to the stress evolution of a multi-crystalline silicon billet during continuous casting. *Int. J. Mater. Res.* **2016**, *107*, 790–800. [[CrossRef](#)]
- Yan, H.; Yue, Q.; Li, Y.; He, J.; Zhong, R. Multiscale residual stress and mechanical behavior analysis in machining of Ti-6Al-4V alloy with advanced microscopic characterization. *J. Manuf. Processes.* **2024**, *120*, 568–578.
- Liu, Y.; Xu, D.; Agmell, M.; Ahadi, A.; Stahl, J.; Zhou, J. Investigation on residual stress evolution in nickel-based alloy affected by multiple cutting operations. *J. Manuf. Processes.* **2021**, *68*, 818–833. [[CrossRef](#)]
- Ji, X.; Liang, Y.S. Model-based sensitivity analysis of machining-induced residual stress under minimum quantity lubrication. *Proc. Inst. Mech. Eng.* **2017**, *231*, 1528–1541. [[CrossRef](#)]
- Jiang, X.; Zhu, Y.; Zhang, Z.; Guo, M.; Ding, Z. Investigation of residual impact stress and its effects on the precision during milling of the thin-walled part. *Int. J. Adv. Manuf. Technol.* **2018**, *97*, 877–892. [[CrossRef](#)]
- Zhang, J.; Lin, B.; Fei, J.; Huang, T.; Xiao, J.; Zhang, X.; Ji, C. Modeling and experimental validation for surface error caused by axial cutting force in end-milling process. *Int. J. Adv. Manuf. Technol.* **2018**, *99*, 327–335. [[CrossRef](#)]
- Huang, K.; Yang, W.Y. Analytical analysis of the mechanism of effects of machining parameter and tool parameter on residual stress based on multivariable decoupling method. *Int. J. Mech. Sci.* **2017**, *128–129*, 659–679. [[CrossRef](#)]
- Jiang, X.; Zhang, Z.; Ding, Z.; Fergani, O.; Liang, S.Y. Tool overlap effect on redistributed residual stress and shape distortion produced by the machining of thin-walled aluminum parts. *Int. J. Adv. Manuf. Technol.* **2017**, *93*, 2227–2242. [[CrossRef](#)]
- Robinson, J.S.; Tanner, D.A.; Truman, C.E.; Wimpory, R.C. Measurement and prediction of machining induced redistribution of residual stress in the Aluminium Alloy 7449. *Exp. Mech.* **2011**, *51*, 981–993. [[CrossRef](#)]

23. Yang, Y.; Fan, L.; Li, L.; Zhao, G.; Han, N.; Li, X.; Tian, H.; He, N. Energy principle and material removal sequence optimization method in machining of aircraft monolithic parts. *Chin. J. Aeronaut.* **2020**, *33*, 2770–2781. [[CrossRef](#)]
24. Zhou, H.; Peng, Z.; Li, G.; Zhou, T.; Wu, H.; Sun, L. A novel genetic-based residual stress and deformation prediction method for the coupled machining process of connecting rod. *Int. J. Adv. Manuf. Technol.* **2024**, *133*, 971–985. [[CrossRef](#)]
25. Guo, M.; Jiang, X.; Ye, Y.; Ding, Z.; Zhang, Z. Investigation of redistribution mechanism of residual stress during multi-process milling of thin-walled parts. *Int. J. Adv. Manuf. Technol.* **2019**, *103*, 1459–1466. [[CrossRef](#)]
26. Cheng, T. Research on the Analysis of Residual Stress in Heat Treatment of Bellows Using ABAQUS. *Materials* **2024**, *17*, 3263. [[CrossRef](#)]
27. Yang, X.-W.; Zhu, J.-C.; Lai, Z.-H.; Liu, Y.; He, D.; Nong, Z.-S. Finite element analysis of quenching temperature field, residual stress and distortion in A357 aluminum alloy large complicated thin-wall workpieces. *Trans. Nonferrous Met. Soc. China* **2013**, *23*, 1751–1760. [[CrossRef](#)]
28. Liu, Z.-W.; Jie, Y.; Li, S.-K.; Nie, W.-J.; Li, L.-X.; Guan, W. Study on inhomogeneous cooling behavior of extruded profile with unequal and large thicknesses during quenching using thermo-mechanical coupling model. *Trans. Nonferrous Met. Soc. China* **2020**, *30*, 1211–1226. [[CrossRef](#)]
29. Dong, Y.B.; Shao, W.Z.; Lu, L.X.; Jiang, J.T.; Zhen, L. Numerical simulation of residual stress in an Al-Cu Alloy block during quenching and aging. *J. Mater. Eng. Perform.* **2015**, *24*, 4928–4940. [[CrossRef](#)]
30. Zhang, Y.-X.; Yi, Y.-P.; Huang, S.-Q.; Dong, F. Influence of quenching cooling rate on residual stress and tensile properties of 2A14 aluminum alloy forgings. *Mater. Sci. Eng. A* **2016**, *674*, 658–665. [[CrossRef](#)]
31. Lu, B.; Lu, X. Evolution of residual stress and distortion of cold-rolled bearing ring from annealing to quenched-tempered heat treatment. *J. Mater. Eng. Perform.* **2018**, *27*, 368–378. [[CrossRef](#)]
32. Kaiser, D.; Damon, J.; Mühl, F.; de Graaff, B.; Kiefer, D.; Dietrich, S.; Schulze, V. Experimental investigation and finite-element modeling of the short-time induction quench-and-temper process of AISI 4140. *J. Mater. Process. Technol.* **2019**, *279*, 116485. [[CrossRef](#)]
33. Li, G.; Xu, H.; Zhou, H.; Jing, X.; Sun, Y. Experimental study of residual stresses of Cam produced by heat treatment and grinding processes. *Int. J. Adv. Manuf. Technol.* **2019**, *100*, 1355–1362. [[CrossRef](#)]
34. Su, X.; Wang, G.; Zhang, Y.T.; Li, J.F.; Rong, Y.M. Modeling on stress evolution of step part for casting-heat treatment processes. *Phys. Procedia* **2013**, *50*, 360–367. [[CrossRef](#)]
35. Tian, G.; Ma, Z.; Zhao, D.; Zhou, H.; Jing, X.; Xie, Z.; Li, G. Research on the dynamic evolution of residual stress in thermal processing of diesel engine blocks based on FEM. *J. Mech. Sci. Technol.* **2021**, *35*, 2419–2430. [[CrossRef](#)]

Disclaimer/Publisher’s Note: The statements, opinions and data contained in all publications are solely those of the individual author(s) and contributor(s) and not of MDPI and/or the editor(s). MDPI and/or the editor(s) disclaim responsibility for any injury to people or property resulting from any ideas, methods, instructions or products referred to in the content.